

# Analyst

Accepted Manuscript



This is an *Accepted Manuscript*, which has been through the Royal Society of Chemistry peer review process and has been accepted for publication.

*Accepted Manuscripts* are published online shortly after acceptance, before technical editing, formatting and proof reading. Using this free service, authors can make their results available to the community, in citable form, before we publish the edited article. We will replace this *Accepted Manuscript* with the edited and formatted *Advance Article* as soon as it is available.

You can find more information about *Accepted Manuscripts* in the [Information for Authors](#).

Please note that technical editing may introduce minor changes to the text and/or graphics, which may alter content. The journal's standard [Terms & Conditions](#) and the [Ethical guidelines](#) still apply. In no event shall the Royal Society of Chemistry be held responsible for any errors or omissions in this *Accepted Manuscript* or any consequences arising from the use of any information it contains.

## ARTICLE

# IR Action Spectroscopy Shows Competitive Oxazolone and Diketopiperazine Formation in Peptides Depends on Peptide Length and Identity of Terminal Residue in the Departing Fragment

Cite this: DOI: 10.1039/x0xx00000x

Received 00th January 2012,

Accepted 00th January 2012

DOI: 10.1039/x0xx00000x

www.rsc.org/

L. J. Morrison,<sup>a</sup> J. Chamot-Rooke<sup>b</sup> and V. H. Wysocki<sup>a</sup>,

The interplay between the entropically and enthalpically favored products of peptide fragmentation is probed using a combined experimental and theoretical approach. These  $b_2$  ion products can take either an oxazolone or diketopiperazine structure. Cleavage after the second amide bond is often a favorable process because the products are small ring structures that are particularly stable. These structures are structurally characterized by action IRMPD spectroscopy and quantified using gas-phase hydrogen-deuterium exchange. The formation of the oxazolone and diketopiperazine has been thought to be largely governed by the *identity* of the first two residues at the N-terminus of the peptide. We show here that the length of the precursor peptide and identity of the *third* residue play a significant role in the formation of the diketopiperazine structure in peptides containing an N-terminal asparagine residue. This is additionally the first instance showing an N-terminal residue with an amide side chain can promote formation of the diketopiperazine  $b_2$  ion structure.

## Introduction

Mass spectrometry and tandem mass spectroscopy have gained increasing popularity as proteomics and structural biology tools in recent years. With the development of soft ionization techniques such as electrospray and nanospray ionization and the ongoing development of different fragmentation techniques, the characterization of protein primary and quaternary structure by tandem mass spectrometry has become increasingly prevalent.<sup>1-9</sup> Collision induced dissociation, or CID, is perhaps the oldest and perhaps most well established of these methods, with extensive effort having gone into the examination of the enthalpic and entropic

factors that define fragmentation in small peptide and non-peptide molecules. One of the principles on which this work is based is known as Rice-Ramsperger-Kassel-Marcus (RRKM) theory, which utilizes both experimental and theoretical data to estimate unimolecular reaction rates.<sup>10</sup> However, this simplistic model fails for large biomolecular systems, as the time scale predicted for the fragmentation of a large protein by RRKM theory far exceeds the analysis time of such a protein in a typical time-of-flight mass spectrometer.<sup>11</sup> Thus, a deeper understanding of the energetics of peptide fragmentation in systems of increasing size is needed to understand the fragmentation behavior of peptides and proteins in mass spectrometry. Here, we utilize a penta-peptide scaffold and the well-studied fragmentation to the  $b_2$  fragment to experimentally

1 probe the interplay between entropic and enthalpic factors in the  
2 fragmentation behavior of peptides.  
3

4 The standard fragmentation pathway of protonated  
5 peptides by CID occurs at the backbone amide bond, generating a  
6 series of “b” and “y” type ions, wherein the C-terminal fragment or y  
7 ion is a truncated peptide and the N-terminal portion forms a cyclic  
8 structure. The smallest b ion, the b<sub>2</sub>, is composed of two residues  
9 and can form either an oxazolone or a diketopiperazine structure.  
10 Both structures are formed by nucleophilic attack on the amide  
11 carbonyl carbon of the second peptide linkage, with the preceding  
12 carbonyl oxygen acting as the nucleophile in the oxazolone pathway  
13 and the N-terminus of the peptide acting as the nucleophile in the  
14 diketopiperazine pathway.<sup>12-13</sup> The diketopiperazine pathway also  
15 requires an isomerization step in which the first amide bond  
16 isomerizes from a trans configuration to a cis configuration prior to  
17 ring closure. This isomerization step adds an interesting chemical  
18 aspect to the formation of b<sub>2</sub> ions: although the diketopiperazine is  
19 typically thermodynamically more stable, trans-cis isomerization  
20 adds a kinetic barrier to the formation of this structure.<sup>14-15</sup> The  
21 typical result is an interplay in which either the thermodynamic  
22 (diketopiperazine) or the kinetic product (oxazolone) is formed,  
23 although the kinetic pathway is typically preferred in CID  
24 experiments.<sup>16-19</sup>  
25

26  
27 A number of studies have shown that residue identity plays  
28 an influential role in favoring the oxazolone or diketopiperazine  
29 pathways. Histidine containing b<sub>2</sub> systems have been extensively  
30 studied, and it has been shown that HA, AH, HG, and GH all form  
31 mixtures of diketopiperazine and oxazolone structures while HP  
32 forms dominantly diketopiperazine.<sup>13,20-21</sup> Wysocki and coworkers  
33 have shown evidence indicating that the diketopiperazine structure is  
34 present in low abundance for the AP, IP, and VP systems and have  
35 rationalized these findings by suggesting that the known higher cis  
36 character of the proline amide bond makes diketopiperazine  
37 formation more favorable.<sup>22-23</sup> The Polfer lab has recently  
38 demonstrated that an arginine residue in the first or second position  
39 also makes diketopiperazine formation competitive in b<sub>2</sub>-H<sub>2</sub>O ions.<sup>24</sup>  
40 Although b<sub>2</sub> ions that contain only aliphatic and aromatic residues  
41 have been shown to feature exclusively oxazolone structures,<sup>25-27</sup> a  
42 basic residue in residue positions 1 or 2 has been shown to allow  
43 diketopiperazine formation.<sup>20,24</sup>  
44

45 In this paper we explore the influence of collision energy  
46 on diketopiperazine and oxazolone formation in NAA and NAXIG  
47 peptide systems using a combination of energy resolved HDX and  
48 action IRMPD spectroscopy. Being only moderately basic, the  
49 asparagine side chain cannot sequester the mobile proton as well as a  
50 strongly basic residue such as arginine, but can still engage in a  
51 number of different proton bridging chemistries as the N-terminal  
52 amino acid.<sup>28</sup> The results show that peptide length and bulk in the  
53 side chain of the third residue has a strong influence on the structure  
54 of the two-residue b<sub>2</sub> fragment that forms following activation by  
55 CID.  
56

## Experimental

### Peptide Synthesis

Fluorenylmethyloxycarbonyl chloride (Fmoc) protected amino acids were obtained from Novabiochem (San Diego, CA) and peptides were synthesized in-house using standard Fmoc solid phase synthesis techniques.<sup>29</sup> The C-terminal, resin-linked residue was used without purification and treated with dimethylformamide (DMF) to swell the polymer bead. The Fmoc protecting group was removed from the growing peptide by washing with 70:30 DMF:piperidine solvent. Coupling was performed in a stepwise manner using -benzotriazole-N,N,N',N'-tetramethyl-uronium-hexafluorophosphate (HBTU) and *N,N*-diisopropylethylamine (DIEA) to promote formation of the amide bond. Peptides were cleaved from the resin by incubation in 95% trifluoroacetic acid and were extracted twice with diethyl ether. Purified peptides were then diluted into 50:50:0.1% Acetonitrile:H<sub>2</sub>O:formic acid electrospray solvent before introduction into the mass spectrometer.

### Mass spectrometry and action IRMPD

Deuterated ammonia was used for all gas-phase hydrogen/deuterium exchange (HDX) studies and was obtained from Sigma-Aldrich (St. Louis, MO). Fragmentation and hydrogen/deuterium exchange studies were performed on a Thermo Scientific (Waltham, MA) Velos Pro dual linear ion trap. Following introduction to the gas phase by an electrospray source, precursor ions were monoisotopically mass selected in the high pressure region of the trap and fragmented by higher-energy collisional dissociation (HCD) to generate the b<sub>2</sub> ions. MS<sup>3</sup> was performed by selecting the b<sub>2</sub> ion population and further fragmenting it by HCD.<sup>30</sup> HCD was performed using normalized collision energies ranging between 10 and 20% for MS<sup>3</sup> studies. Thermo Scientific expresses HCD as a relative percentage value and the actual voltages used in the instrument are proprietary and therefore unknown. For this reason, HCD energy will be expressed as a percentage. Gas-phase hydrogen/deuterium exchange (HDX) was performed by saturating the trap with deuterated ammonia and subsequently flushing with helium to generate a low ambient pressure of deuterated ammonia that remained relatively constant for several minutes. The exchange of leucine-enkephalin for 10 ms was used to monitor this pressure and incubation of the analyte b<sub>2</sub> ions was performed in triplicate in all experiments for 2 minute intervals using a deuterated ammonia pressure that resulted in 5% exchange of leucine-enkephalin.

Action IRMPD spectroscopy was performed using a Bruker Esquire 3000+ ion trap coupled to a free electron laser at the CLIO facility in Orsay, France.<sup>31-32</sup> Ions were introduced to the gas phase by electrospray ionization and protonated precursor molecules transmitted to the ion trap for CID and IRMPD. Precursor ions of sequence NAA, and NAXIG (X = alanine (A), aminobutyric acid

(Abu), valine (V) and tert-butyl glycine (tbG)) were mass selected and fragmented within the ion trap to generate  $b_2$  ions. MS<sup>4</sup> experiments, in which the  $b_2$ -NH<sub>3</sub> fragment was irradiated by the FEL laser, were performed by generating the NAAIG  $b_2$  ion by trap CID, isolating it in the trap, and further activating it by trap CID. Once generated,  $b_2$  and  $b_2$ -NH<sub>3</sub> ions were isolated respectively, and subjected to 180 ms pulses of irradiation from the free electron laser, with pulses comprised of four, 10  $\mu$ s macropulses spaced by 40 ms intervals. Each macropulse was composed of 8 micropulses, each lasting one picosecond and spaced by 16 ns intervals. Typical laser powers were 450-600 mW at 1500 cm<sup>-1</sup>. Irradiation of the laser results in fragmentation of the  $b_2$  or  $b_2$ -NH<sub>3</sub> ion if the frequency of the laser is equal to an IR absorption band of the ion. Following irradiation at each frequency, fragment and precursor ions were detected using the ion trap analyzer. Spectra were generated by either plotting the total fragmentation efficiency of the  $b_2$  or  $b_2$ -NH<sub>3</sub> ion against irradiation frequency. Because the oxazolone and diketopiperazine structures often fragment differently, fragmentation efficiency can alternatively be considered with regard to a single fragment, giving IRMPD spectra reflecting a single structure if the fragment is unique to the structure. The fragmentation efficiency of the  $b_2$  ion will be presented in some cases by considering separately the  $b_2$ -CO and  $b_2$ -NH<sub>3</sub> fragments.

## Computations

Optimizations and frequency calculations were performed using the Gaussian 09 software package with a B3LYP/6-311++G\*\* basis set.<sup>33</sup> Preliminary conformations of  $b_2$  oxazolone and diketopiperazine structures were obtained using a conformation search function within the MacroModel software package.<sup>34</sup> Collections of conformations were generated for both the diketopiperazine and oxazolone classes of molecules, considering all amine nitrogens, amide oxygens, and the asparagine side chain amide nitrogen as potential protonation sites. Redundant conformers were eliminated at the B3LYP/6-31G level if they shared identical bridging with another conformer and were greater than 50 kJ/mol higher in energy than the lowest energy conformer. Frequency spectra were scaled by 0.978 and the full-width at half-maximum peak width adjusted to 10 cm<sup>-1</sup> to best correlate with experimental spectra. The same approach was used for the  $b_2$ -NH<sub>3</sub> structures, following formation of the oxazolone or diketopiperazine  $b_2$ -NH<sub>3</sub> by the suggested mechanisms shown in Supporting Information, Figure S1. Calculations of this type were also performed on AlaAsn succinimide and imino- $\gamma$ -butyrolactone structures and the energies and frequency spectra associated with these rearranged structures are shown in Supporting Information, Figure S2.

## Results and Discussion

### Comparison of the $b_2$ ion population from NAA, NAAIG, and NAVIG

Peptides featuring an N-terminal asparagine or glutamine have been shown previously by Stein and coworkers to fragment via abundant water and ammonia loss pathways.<sup>35-36</sup> The fragmentation behavior of the  $b_2$  ion from NAA, NAAIG, and NAVIG by CID is

consistent with their findings (Figure 1). The  $b_2$  ions from these precursors exhibit largely the same fragments at  $m/z$  169 ( $b_2$ -NH<sub>3</sub>), 158 ( $b_2$ -CO,  $a_2$ ), and 141 ( $b_2$ -CO-NH<sub>3</sub>), representative of two major fragmentation pathways: ammonia loss, CO loss to form the  $a_2$  ion, and a combination of the two. The intensities of the CO loss and ammonia loss fragments differ in each of the three spectra, however, suggesting that the  $b_2$  ions may have different structures. Action IRMPD was therefore used to probe these  $b_2$  ions, with the assumption that mixtures of structures might be present for these  $b_2$  ions.

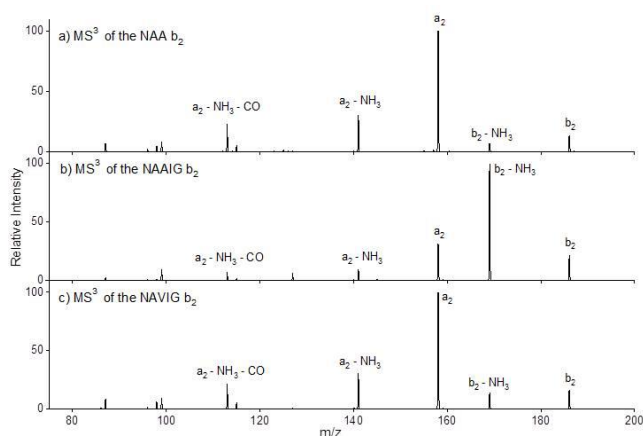


Figure 1: MS<sup>3</sup> of the  $b_2$  ions of (a) NAA, (b) NAAIG, and (c) NAVIG using HCD to fragment the precursor and the subsequent  $b_2$  ion population, respectively. The  $b_2$  ions of NAVIG and NAAIG were generated using 20% HCD energy and the  $b_2$  ion from NAA was generated using 12.5% HCD energy in order to compensate for its smaller size. The  $b_2$  populations from all precursors were fragmented using 10% HCD collision energies.

Action IRMPD spectra were obtained for the  $b_2$  ions from singly charged peptides with sequence NAA, NAAIG, and NAVIG. The  $b_2$  ion action IRMPD spectra from these analogues are shown in Figure 2 (a) – (c). From inspection of the experimental IRMPD spectra from NAA and NAAIG, clear differences in the  $b_2$  absorption behavior are evident in the 1500-2000 cm<sup>-1</sup> range, suggesting that at least two different structures exist for the NA  $b_2$  ion. These spectra suggest that the type of  $b_2$  ion structure that forms is strongly related to the length of the precursor peptide. Inspection of the action IRMPD spectrum of the  $b_2$  ion from NAVIG shows that it contains features observed in both the NAA and NAAIG experimental  $b_2$  spectra, suggesting the  $b_2$  population from this analogue could be a mixture of the two structures and indicating the influence of the third residue on  $b_2$  ion structure. Dashed red and dashed blue overlays are shown in Figure 2(c) and were generated by considering only the carbon monoxide loss and ammonia loss peaks from the NAVIG  $b_2$  ion, respectively. The dashed blue trace (ammonia loss) is observed to share the same bands as the action IRMPD spectrum of NAAIG and the dashed red trace agrees very well with the NAA experimental  $b_2$  spectrum. Thus, treatment of the data in this way allows a clear separation of the IRMPD spectra of the two different isomers.

The  $b_2$  population from NAAIG exhibits dominant absorption bands at 1280, 1420, 1600, and 1750  $\text{cm}^{-1}$  while the  $b_2$  population from NAA features dominant absorption bands at 1610 and 1690, as well as a weak band at 1900  $\text{cm}^{-1}$ . Bands in the relatively high range of approximately 1900  $\text{cm}^{-1}$  are typically thought to correspond to a ring carbonyl stretching mode and are often considered diagnostic of an oxazolone structure. Laser power in this range is relatively weak ( $\approx 210\text{--}250$  mW) and this band typically appears lower in intensity than predicted by DFT calculations. Nonetheless, the IRMPD spectrum for the  $b_2$  ion of NAA can be seen to be in excellent agreement with the calculated IR spectrum of the ring protonated oxazolone structure shown in Figure 2(d). This is in agreement with recent work published by Grzetic and Oomens, in which they also found that the  $b_2$  ion from NAA was an oxazolone structure.<sup>37</sup> Although it is typical for the intensity of peaks in action IRMPD spectra to be quite different than in the predicted IR spectra, the relative intensity of the bands at 1420, 1610, and 1690  $\text{cm}^{-1}$  agree very well with theory. The predicted spectrum of the lowest energy diketopiperazine structure, however, is in poorer agreement with the experimental  $b_2$  spectrum from the NAAIG peptide. Higher energy diketopiperazine structures and AlaAsn succinimide and imino- $\gamma$ -butyrolactone structures also match poorly with the experimental spectrum (see Supporting Information Figure S2). Although theory predicts several diketopiperazine vibrational modes at 1450 (ring amide II), 1625 ( $\text{NH}_2$  scissor), and 1750  $\text{cm}^{-1}$  (ring amide I) that agree relatively well in position with the intense absorption modes observed experimentally, several bands predicted by theory (1200, 1510, and 1800  $\text{cm}^{-1}$ ) are not observed in the experimental spectrum. Moreover, the intensity of the strong bands in the experimental spectrum does not correlate well with the predicted spectrum. For this reason, it is not possible to confidently assign the  $b_2$  population from NAAIG as a diketopiperazine. Action IRMPD suggests, however, that NAA dominantly forms an oxazolone  $b_2$  ion structure, NAAIG dominantly forms a second  $b_2$  ion structure, and NAVIG forms a mixture of the two.

One reason that theory seems to poorly predict the diketopiperazine structure of the NA  $b_2$  ion is due to the asparagine side chain. Because of its length, it can bridge and stabilize the mobile proton in a variety of different conformations depending on the dihedral angle of the side chain. Small shifts in this angle result in dramatic red and blue shifting of the predicted absorption modes. This effect is also likely related to multiple photons being absorbed in action IRMPD experiments, in which small structural changes, such as the shifting of this side chain, occur following absorption of the first photon. Thus, in order to circumvent multi-photon effects and the influence of the “floppy” side chain, action IRMPD was performed on the  $b_2\text{-NH}_3$  fragment from the  $b_2$  of NAAIG. If a diketopiperazine is present as a  $b_2$  structure, nucleophilic attack from the diketopiperazine ring carbonyl oxygen on the side chain amide carbonyl carbon will result in the closure of a five-membered ring and ammonia loss. An analogous pathway is available for the oxazolone structure, in which the ring nitrogen acts as the nucleophile (see Supporting Information, Figure S1 for the proposed mechanism). The advantage of these two structures is that they are both rigid double ring structures with limited conformational flexibility (see structures in Figure 3). Because the

diketopiperazine and oxazolone structures are not known to interconvert, the  $b_2\text{-NH}_3$  structure is a direct reflection of the  $b_2$  population and should confirm whether the diketopiperazine structure is present in the  $b_2$  ion population. The  $b_2\text{-NH}_3$  population from NAAIG was generated by fragmenting NAAIG by trap CID in  $\text{MS}^2$  and further isolating and fragmenting the  $b_2$  population in  $\text{MS}^3$ . The experimental action IRMPD spectrum of this  $b_2\text{-NH}_3$  population is shown in Figure 3(a) and the theoretical diketopiperazine- $\text{NH}_3$  and oxazolone- $\text{NH}_3$  are shown in Figure 3(b) and (c), respectively. The inset of Figure 3(a) shows the range of 1850–2000  $\text{cm}^{-1}$ , which was acquired using a laser power higher than typical in this range (450 mW). From inspection, the agreement between the experimental and the calculated spectra for diketopiperazine  $b_2\text{-NH}_3$  can be seen to be very good, with excellent agreement of the amide II mode at 1700 and amide I mode 1790  $\text{cm}^{-1}$ . In the high power scan, additional agreement can be seen in the ring ester carbonyl vibrational mode that appears at 1900  $\text{cm}^{-1}$ . The IRMPD spectrum of the  $b_2\text{-NH}_3$  formed from the  $b_2$  of NAAIG confirms that the other structure observed in the  $b_2$  populations of the NAAIG and NAVIG analogues is in fact a diketopiperazine. This is the first example of diketopiperazine formation in systems lacking a basic residue or a proline. Moreover, it is the first evidence to show that peptide length and third residue identity directly influence the  $b_2$  ion structure that forms.

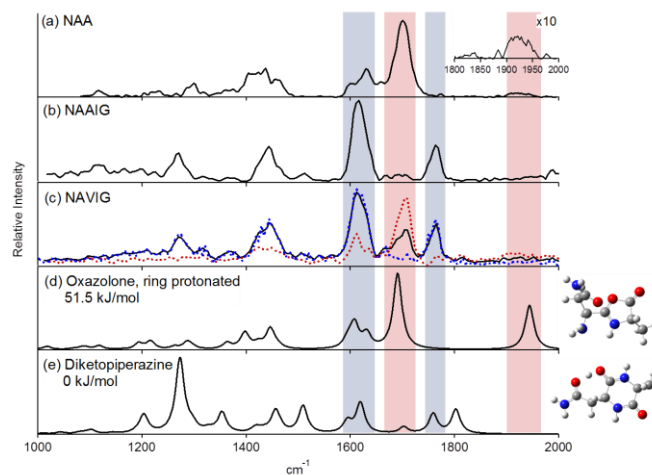


Figure 2: Experimental action IRMPD spectra of the  $b_2$  populations of (a) NAA, (b) NAAIG, and (c) NAVIG. The theoretical IR spectrum for the ring protonated oxazolone is shown in (d) and the theoretical spectrum for the diketopiperazine is shown in (e). Red (maxima at 1610 and 1690  $\text{cm}^{-1}$ ) and blue (maxima at 1610 and 1750  $\text{cm}^{-1}$ ) dashed traces in (c) show the action IRMPD spectrum from the  $b_2$  population of NAVIG generated by separately considering the CO loss (red) and  $\text{NH}_3$  loss (blue) peaks respectively.

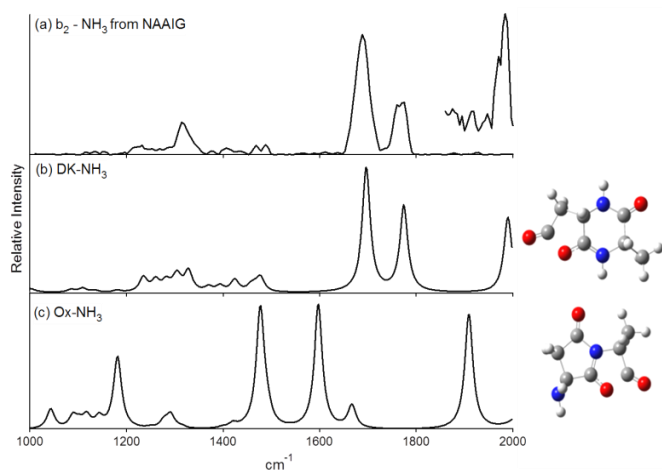


Figure 3: Experimental action IRMPD spectrum of the  $b_2$ -NH<sub>3</sub> from NAAIG is shown in (a), the theoretical IR spectrum of the diketopiperazine-NH<sub>3</sub> is shown in (b), and the theoretical IR spectrum of the oxazolone-NH<sub>3</sub> is shown in (c). The inset in (a) shows the range of 1850-2000 cm<sup>-1</sup> that was recorded using a higher power of the FEL laser in that range (450 mW).

### Examination of the third residue effect: IRMPD and HDX of NAXIG analogues

In order to better understand the role of the third residue on  $b_2$  ion formation, action IRMPD and hydrogen-deuterium exchange (HDX) were performed on the  $b_2$  population from NAXIG pentapeptides, wherein X was aminobutyric acid (Abu) and tert-butyl glycine (tbG) in addition to alanine (A) and valine (V). The left panel of Figure 4 shows the action IRMPD spectra of the  $b_2$  ions from these analogues. As discussed above, the action IRMPD spectrum of the  $b_2$  ion from NAAIG features dominant bands at 1420, 1600, and 1750 cm<sup>-1</sup> that correspond to the diketopiperazine structure. As the branching chemistry of the side chain of the third residue is sequentially increased from a methyl group (A), to an ethyl (Abu), to an isopropyl (V), to a tert-butyl (tbG), the NH<sub>2</sub> scissoring mode of the oxazolone (1690 cm<sup>-1</sup>), the most dominant band in the oxazolone spectrum, can be seen to increase in intensity. More bulk in the side chain of the third residue thus shifts the  $b_2$  population towards the oxazolone structure. However, because action IRMPD is known to be poorly suited to estimating relative population abundances of isomers, gas phase HDX following activation of the precursor peptide at different collision energies (ER-HDX) was performed on the  $b_2$  populations of the four NAXIG analogues, and is shown in the right panel of Figure 4. A single population, centered at  $D_0$ , is observed for the  $b_2$  from NAAIG and NA(Abu)IG. In contrast, at least two distinct populations are observed in the HDX distributions of the  $b_2$  ions from NAVIG and NA(tbG)IG, one dominated by  $D_0$ , and a second centered at  $D_2$ . Although the oxazolone and the diketopiperazine structures both have 5 exchangeable protons, the slow exchanging population can be assigned to the diketopiperazine because all five of the protons are amide protons, which are known to exchange more slowly than the protons from acidic or basic groups.<sup>20,23,38</sup> In contrast, the oxazolone structure contains two amide protons, two amine protons,

and one imine proton; thus, it is expected to rapidly exchange 2-3 protons with ND<sub>3</sub>, consistent with the second population. HDX is therefore in excellent agreement with the action IRMPD data, in which the NA  $b_2$  population from NAAIG and NA(Abu)IG appeared to be dominantly diketopiperazine, and a mixture of oxazolone and diketopiperazine when generated from NAVIG and NA(tbG)IG.

In order to understand the how energy impacts the formation of the diketopiperazine and oxazolone structures, it is necessary to examine the ER-HDX data for each analogue. HDX spectra were collected in triplicate and these data are summarized in Figure 5 as a function of diketopiperazine abundance (see Figure 4 for representative exchange patterns). The population abundance of the oxazolone and diketopiperazine isomers was estimated by fitting the HDX distribution to Poisson functions and manually parameterizing the fits. Typical variances for these fits were less than 0.001. This approximation is by no means an exact representation of the oxazolone and diketopiperazine populations, but is useful for tracking relative abundance of the two populations as a function of collision energy. With the exception of the  $b_2$  from NAA, all  $b_2$  populations exhibit a decrease in diketopiperazine abundance (and therefore an increase in oxazolone abundance) as collision energy is increased. The increase in  $b_2$  diketopiperazine abundance in the NAA system clearly indicates that the energetics of the oxazolone and diketopiperazine pathways are different in the tripeptide analogue compared with the pentapeptide analogues. The  $b_2$  diketopiperazine abundance as a function of energy can be well fit to parabolic functions, with NAAIG and NA(Abu)IG having convex curvature and NAVIG and NA(tbG)IG having a concave curvature. This curvature is interesting and may be a reflection of the interplay of enthalpy and entropy, but because the full thermodynamics of these transition states are not known, it is difficult to say with any certainty why the curvature is present. It is interesting to note the change in behavior of the  $b_2$  population as the side chain of the third residue is changed from an ethyl group to an isopropyl (Abu to V), as the slope and curvature of the  $b_2$  diketopiperazine abundance versus energy relationship dramatically changes between these residues. This behavior suggests that the structure and shape of the isopropyl side chain is particularly significant to the energy barriers along the oxazolone and diketopiperazine pathways, and that the presence of branching groups plays a particularly important role in these pathways.

The observed decrease in diketopiperazine abundance as a function of increasing collision energy is unusual because the diketopiperazine structure is calculated to be 51.5 kJ/mol lower in energy than the oxazolone structure. In addition, the ring closure and dissociation barriers of the diketopiperazine from GG and GGG have been shown to be significantly higher than these barriers for the oxazolone structure.<sup>15,18</sup> Thus, the diketopiperazine structure is typically thought to be the thermodynamic product and form at higher collision energies than the oxazolone, even though the energetic difference between the two structures is relatively small. This line of reasoning seems to support the data for the NAA system, in which slightly more diketopiperazine ( $\approx 5\%$  increase) seems to form at the highest collision energies. One explanation for more abundant

1 diketopiperazine at low energies in the pentapeptide systems is that  
 2 the oxazolone structure is entropically favored over the  
 3 diketopiperazine due to the differences in closing a five vs. a six  
 4 membered ring. In terms of transition state barriers, this suggests that  
 5 the highest barrier to the formation of the diketopiperazine, be it ring  
 6 closure, trans-cis isomerization, or dissociation, must be lower in  
 7 energy than the highest energy barrier for the formation of the  
 8 oxazolone structure, presumably the ring closure barrier. However,  
 9 because closure of a five-membered ring is more entropically  
 10 favorable, the oxazolone ring closure transition state must be looser  
 11 than the diketopiperazine transition state; the density of states at these  
 12 saddle points therefore allows oxazolone formation to be competitive  
 13 with diketopiperazine formation at high collision energies. Figure 6  
 14 shows a diagram describing this reasoning.

15  
 16 It is clear from an energetic perspective that the relative  
 17 energies and tightness of the oxazolone and diketopiperazine  
 18 transition states play a critical role in favoring oxazolone or  
 19 diketopiperazine formation. However, the direct role of the side chain  
 20 of the third residue in the peptide system on the relative energies of  
 21 these barriers is less obvious. It is appealing to consider this problem  
 22 in terms of backbone rotational freedom, as the more bulky side chains  
 23 undoubtedly limit the rotational space of the backbone psi and phi  
 24 dihedral angles. From this perspective, it is straightforward to propose  
 25 a mechanism in which the more bulky side chains, that is, valine and  
 26 tert-butyl glycine, restrict backbone torsional angles such that certain  
 27 proton bridges are disfavored or altogether impossible. It is possible  
 28 that the absence or presence of such interactions would favor or  
 29 disfavor certain fragmentation pathways. However, the precise  
 30 interactions, particularly those related to the trans-cis isomerization  
 31 and ring closure transition states, require extensive computational  
 32 modeling of the precursor peptides and fragmentation intermediates  
 33 such as the  $b_4$  ion and is beyond the scope of this paper. Nonetheless,

34  
 35 it is clear that peptide composition and length play a significant role  
 36 in the formation of  $b_2$  fragment ion structures in systems containing  
 37 an N-terminal asparagine.

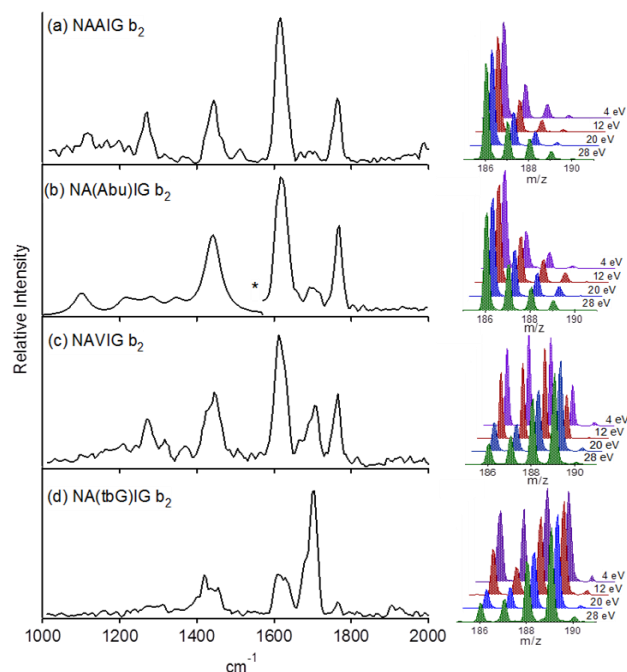


Figure 4: Left: action IRMPD of the  $b_2$  population from (a) NAAIG, (b) NA(Abu)IG, (c) NAVIG, and (d) NA(tbG)IG. Right (a)-(d): ER-HDX of the  $b_2$  ion from NAAIG, NA(Abu)IG, NAVIG, and NA(tbG)IG, respectively. \* Due to laser failure, action IRMPD spectrum was acquired in two segments. A similar series of spectra, obtained using higher-energy source conditions, is shown in Supporting Information Figure S3.

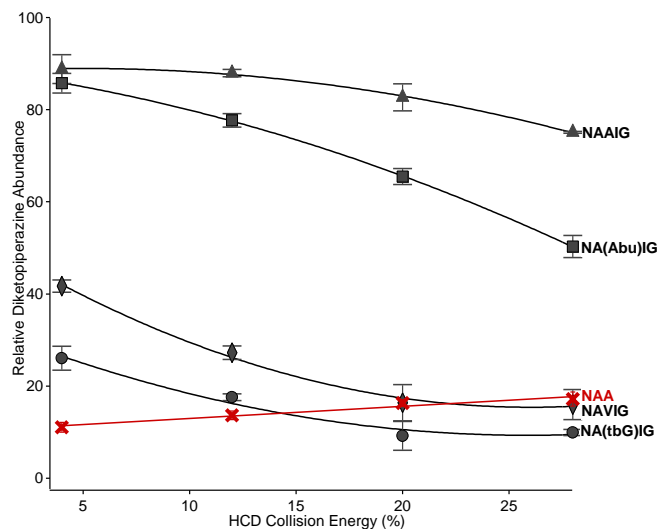


Figure 5: Relative abundance of the  $b_2$  diketopiperazine population from NAAIG (triangles), NA(Abu)IG (squares), NAVIG (diamonds), NA(tbG)IG (circles), and NAA (Xs) as a function of the HCD collision energy used to generate the  $b_2$  population.

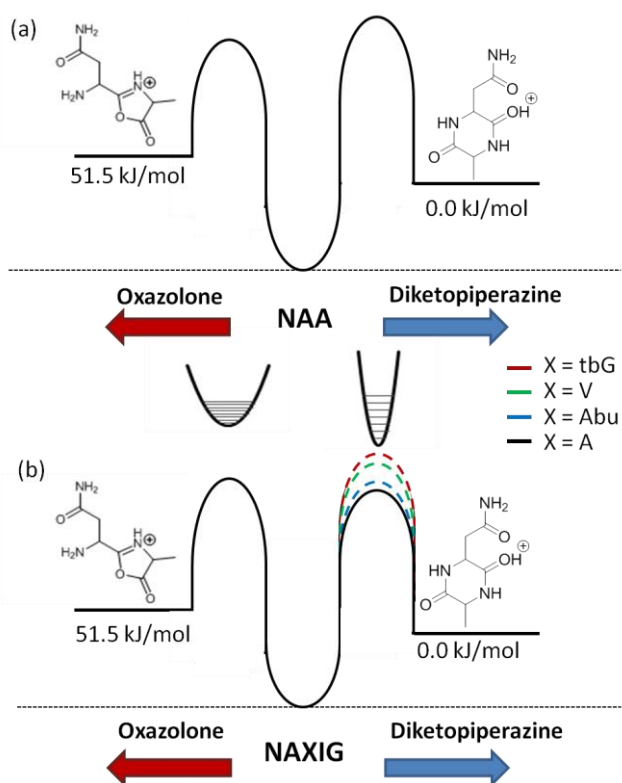


Figure 6: Diagram showing estimated ring closure barriers for the formation of oxazolone and diketopiperazine  $b_2$  ion structures for (a) NAA and (b) NAXIG based on ER-HDX data and computational modeling of NA  $b_2$  oxazolone and diketopiperazine structures.

## Conclusions

Action IRMPD of the  $b_2$  population of NAA, NAAIG, NA(Abu)IG, NAVIG, and NA(tbG)IG shows the presence of at least two isomeric  $b_2$  structures. Action IRMPD of the  $b_2$ -NH<sub>3</sub> from the  $b_2$  of NAAIG and computational modeling allow these two structures to be assigned as a ring protonated oxazolone and a ring carbonyl oxygen protonated diketopiperazine. This is the first instance of diketopiperazine formation in a peptide without a basic residue or a proline. Moreover, the bulk of the third residue and peptide length are additionally shown for the first time to be factors in oxazolone vs. diketopiperazine formation. Energy resolved HDX suggests that the relative energy and tightness of the oxazolone and diketopiperazine transition states are critical factors along these two pathways. Changes in trendlines relating diketopiperazine abundance to collision energy suggests the presence of a branching group in the third position of the pentapeptide causes the oxazolone pathway to be favored. This is in direct contrast to the pentapeptide systems containing only a methyl or an ethyl group in this position, as these analogues strongly favor the diketopiperazine structure. A systematic study varying the length and chemical identity of the first and third residues and more

extensive modeling of transition states is necessary to more fully understand the mechanistic details of this behavior.

## Acknowledgements

Professor Anne McCoy is acknowledged for her assistance in interpreting multi-photon effects in the action IRMPD spectra. This research is supported by NIH R01 51387 to Dr. Wysocki and Ohio State University. The authors thank the CLIO team (J. M. Ortega, C. Six, G. Perilhous, J. P. Berthet) as well as P. Maître and V. Steinmetz for their support during the experiments. The research leading to these results has received funding from the European Union's Seventh Framework Program (FP7/2007-2013) under grant agreement number 226716.

## Notes and references

<sup>a</sup> Department of Chemistry and Biochemistry  
The Ohio State University  
484 W. 12th Ave, Columbus, OH 43210

<sup>b</sup> Pasteur Institute  
28 Rue du Docteur Roux  
75724 PARIS Cedex 15

Electronic Supplementary Information (ESI) available: [details of any supplementary information available should be included here]. See DOI: 10.1039/b000000x/

- (1) Florance, H. V.; Stopford, A. P.; Kalapothakis, J. M.; McCullough, B. J.; Bretherick, A.; Barran, P. E. *Analyst* **2011**, *136*, 3446.
- (2) Jarrold, M. F. *Phys. Chem. Chem. Phys.* **2007**, *9*, 1659.
- (3) Oh, H.; Breuker, K.; Sze, S. K.; Ge, Y.; Carpenter, B. K.; McLafferty, F. W. *Proceedings of the National Academy of Sciences* **2002**, *99*, 15863.
- (4) Bleiholder, C.; Dupuis, N. F.; Wyttenbach, T.; Bowers, M. T. *Nat Chem* **2011**, *3*, 172.
- (5) Katta, V.; Chait, B. T. *J. Am. Chem. Soc.* **1991**, *113*, 8534.
- (6) Sharon, M. *J. Am. Soc. Mass Spectrom.* **2010**, *21*, 487.
- (7) Taverner, T.; Hernandez, H.; Sharon, M.; Ruotolo, B. T.; Matak-Vinkovic, D.; Devos, D.; Russell, R. B.; Robinson, C. V. *Acc. Chem. Res.* **2008**, *41*, 617.
- (8) Tolmachev, A. V.; Robinson, E. W.; Wu, S.; Pasa-Tolic, L.; Smith, R. D. *Int. J. Mass Spectrom.* **2009**, *287*, 32.
- (9) Zhou, M.; Huang, C.; Wysocki, V. H. *Anal. Chem. (Washington, DC, U. S.)* **2012**, *84*, 6016.
- (10) Wardlaw, D. M.; Marcus, R. A. *Chemical Physics Letters* **1984**, *110*, 230.
- (11) Griffin, L. L.; McAdoo, D. J. *Journal of the American Society for Mass Spectrometry* **1993**, *4*, 11.
- (12) Paizs, B.; Suhai, S. *Mass Spectrometry Reviews* **2005**, 508.
- (13) Perkins, B. R.; Chamot-Rooke, J.; Yoon, S. H.; Gucinski, A. C.; Somogyi, A.; Wysocki, V. H. *Journal of the American Chemical Society* **2009**, 17528.
- (14) Balta, B.; Aviyente, V.; Lifshitz, C. *J. Am. Soc. Mass Spectrom.* **2003**, *14*, 1192.
- (15) Armentrout, P. B.; Heaton, A. L. *J. Am. Soc. Mass Spectrom.* **2012**, *23*, 632.
- (16) Yalcin, T.; Csizmadia, I. G.; Peterson, M. R.; Harrison, A. G. *J. Am. Soc. Mass Spectrom.* **1996**, *7*, 233.

- 1  
2  
3  
4  
5  
6  
7  
8  
9  
10  
11  
12  
13  
14  
15  
16  
17  
18  
19  
20  
21  
22  
23  
24  
25  
26  
27  
28  
29  
30  
31  
32  
33  
34  
35  
36  
37  
38  
39  
40  
41  
42  
43  
44  
45  
46  
47  
48  
49  
50  
51  
52  
53  
54  
55  
56  
57  
58  
59  
60
- (17) Polfer, N. C.; Oomens, J.; Suhai, S.; Paizs, B. *J. Am. Chem. Soc.* **2005**, *127*, 17154.
- (18) Paizs, B.; Suhai, S. *Rapid Commun. Mass Spectrom.* **2002**, *16*, 375.
- (19) Nold, M. J.; Wesdemiotis, C.; Yalcin, T.; Harrison, A. G. *Int. J. Mass Spectrom. Ion Processes* **1997**, *164*, 137.
- (20) Gucinski, A. C.; Chamot-Rooke, J.; Nicol, E.; Somogyi, A.; Wysocki, V. H. *J. Phys. Chem. A* **2012**, *116*, 4296.
- (21) Farrugia, J. M.; Taverner, T.; O'Hair, R. A. J. *Int. J. Mass Spectrom.* **2001**, *209*, 99.
- (22) Smith, L. L.; Herrmann, K. A.; Wysocki, V. H. *J. Am. Soc. Mass Spectrom.* **2006**, *17*, 20.
- (23) Gucinski, A. C.; Chamot-Rooke, J.; Steinmetz, V.; Somogyi, A.; Wysocki, V. H. *J. Phys. Chem. A* **2013**, *117*, 1291.
- (24) Zou, S.; Oomens, J.; Polfer, N. C. *Int. J. Mass Spectrom.* **2012**, *316-318*, 12.
- (25) Oomens, J.; Young, S.; Molesworth, S.; van Stipdonk, M. *Journal of the American Society for Mass Spectrometry* **2009**, *20*, 334.
- (26) Bythell, B.; Somogyi, Á.; Paizs, B. *Journal of the American Society for Mass Spectrometry* **2009**, *20*, 618.
- (27) Yoon, S. H.; Chamot-Rooke, J.; Perkins, B. R.; Hilderbrand, A. E.; Poutsma, J. C.; Wysocki, V. H. *Journal of the American Chemical Society* **2008**, *130*, 17644.
- (28) Bouchoux, G. *Mass Spectrometry Reviews* **2012**, *31*, 391.
- (29) *Solid-Phase Peptide Synthesis: A Practical Approach*; Atherton, E.; Sheppard, R. C., Eds.; Oxford University Press: Oxford, 1989.
- (30) Olsen, J. V.; Macek, B.; Lange, O.; Makarov, A.; Horning, S.; Mann, M. *Nat Meth* **2007**, *4*, 709.
- (31) Simon, A.; Jones, W.; Ortega, J.-M.; Boissel, P.; Lemaire, J.; Maitre, P. *J Am Chem Soc* **2004**, *126*, 11666.
- (32) Maitre, P.; Le Caër, S.; Simon, A.; Jones, W.; Lemaire, J.; Mestdagh, H.; Heninger, M.; Mauclair, G.; Boissel, P.; Prazeres, R.; Glotin, F.; Ortega, J.-M. *Nuclear Instruments and Methods in Physics Research Section A: Accelerators, Spectrometers, Detectors and Associated Equipment* **2003**, *507*, 541.
- (33) Gaussian, I.; 09 ed.; Frisch, M. J. T., G. W.; Schlegel, H. B.; Scuseria, G. E.; Robb, M. A.; Cheeseman, J. R.; Scalmani, G.; Barone, V.; Mennucci, B.; Petersson, G. A.; Nakatsuji, H.; Caricato, M.; Li, X.; Hratchian, H. P.; Izmaylov, A. F.; Bloino, J.; Zheng, G.; Sonnenberg, J. L.; Hada, M.; Ehara, M.; Toyota, K.; Fukuda, R.; Hasegawa, J.; Ishida, M.; Nakajima, T.; Honda, Y.; Kitao, O.; Nakai, H.; Vreven, T.; Montgomery, Jr., J. A.; Peralta, J. E.; Ogliaro, F.; Bearpark, M.; Heyd, J. J.; Brothers, E.; Kudin, K. N.; Staroverov, V. N.; Kobayashi, R.; Normand, J.; Raghavachari, K.; Rendell, A.; Burant, J. C.; Iyengar, S. S.; Tomasi, J.; Cossi, M.; Rega, N.; Millam, J. M.; Klene, M.; Knox, J. E.; Cross, J. B.; Bakken, V.; Adamo, C.; Jaramillo, J.; Gomperts, R.; Stratmann, R. E.; Yazyev, O.; Austin, A. J.; Cammi, R.; Pomelli, C.; Ochterski, J. W.; Martin, R. L.; Morokuma, K.; Zakrzewski, V. G.; Voth, G. A.; Salvador, P.; Dannenberg, J. J.; Dapprich, S.; Daniels, A. D.; Farkas, Ö.; Foresman, J. B.; Ortiz, J. V.; Cioslowski, J.; Fox, D. J., Ed. Wallingford, CT, 2009.
- (34) Schrödinger, L.; 9.9 ed. New York, NY, 2011.
- (35) Godugu, B.; Neta, P.; Simon-Manso, Y.; Stein, S. E. *J. Am. Soc. Mass Spectrom.* **2010**, *21*, 1169.
- (36) Neta, P.; Pu, Q.-L.; Kilpatrick, L.; Yang, X.; Stein, S. E. *J. Am. Soc. Mass Spectrom.* **2007**, *18*, 27.
- (37) Grzetic, J.; Oomens, J. *J. Am. Soc. Mass Spectrom.* **2013**, *24*, 1228.
- (38) Pan, J.; Heath, B. L.; Jockusch, R. A.; Konermann, L. *Anal. Chem. (Washington, DC, U. S.)* **2012**, *84*, 373.

Diketopiperazine formation in gas-phase peptides on the side-chain of the third residue

